Transverse Heterogeneity in PET Fibers

D. W. TOMLIN,[1] C. M. ROLAND,[1] and L. I. SLUTSKER[2]

[1]Chemistry Division, Code 6120, Naval Research Laboratory, Washington, DC 20375-5000; and [2]Research and Development Center, Amoco Fabrics and Fibers Co., P. O. Box 43288, Atlanta, Georgia 30336

SYNOPSIS

X-ray scattering from a series of poly(ethylene terephthalate) (PET) fibers spun at different speeds is analyzed to probe the morphology in the direction transverse to the fiber axis. Both the apparent crystal modulus, determined from the change in wide-angle X-ray scattering angle with fiber stretching, and the transverse degree of crystallinity indicate there is a substantial interfibrillar amorphous content. In the PET fiber spun at conventional speeds, only roughly one-quarter of the fiber cross-section is actually occupied by fibrils. The transverse crystallinity increases for fibers spun at speeds sufficient to cause crystallization in the spin line. The X-ray moduli and fibril diameters are correspondingly larger in these high speed spun fibers. © 1993 John Wiley & Sons, Inc.

Keywords: poly(ethylene terephthalate) • transverse heterogeneity • crystallinity • high speed spinning

INTRODUCTION

The most obvious morphological feature of fibers made from PET is the alternating crystalline and amorphous regions along the fiber direction. Hence, analyses of structure-mechanical property relationships usually focus on this fibrillar morphology, although the behavior of the fibers cannot be reconciled solely in terms of the longitudinal structure. The experiments described herein were undertaken to assess the significance of transverse heterogeneity in PET fibers.

EXPERIMENTAL

The PET fibers (1000 denier = 0.08 mm^2 cross-sectional area) were obtained from the Industrial Fibers Division of Allied-Signal Corporation. Sample designations, given in Table I, are the same used in reports from other laboratories.[1-3] The yarns were spun at increasing take-up speeds ranging from conventional spinning to the range associated with high-speed spinning (HSS).[4] All fibers were drawn to 95% of their maximum draw ratio (85% for the EXP fiber), followed by similar heat treatment to yield the morphological characteristics given in Table I. The fibers spun at the higher speeds all exhibit characteristics of HSS yarns (e.g., crystallization in the spin line).[1-3]

The change in the unit-cell dimensions was measured from the change in wide-angle X-ray scattering angle of the fibers upon stretching. PET crystals have a triclinic unit cell, with the c axis in the draw direction of the fiber.[5,6] There is no (001) reflection in PET; however, the $(\bar{1}05)$ planes, reflecting at $2\theta = 43°$, can be taken as approximately parallel to the c axis of the polymer.[7] Stresses up to about 90 MPa were applied to a fiber, after which it was allowed to relax for 900 s before the angle of the $(\bar{1}05)$ peak was measured. Results herein are averages of four separate measurements made at each stress. There was no change in lineshape with stress, indicating no significant change in crystal orientation in the drawn fibers.

The wide-angle X-ray scattering (WAXS) measurements were performed at the Materials Laboratory of the Wright Research and Development Center at Wright-Patterson Air Force Base. The experimental arrangement used for these experiments is described elsewhere.[8,9] The X-ray source was a Rigaku Rotoflex RU-200 with copper anode (λ = 1.542 Å) operated at 45 kV and 70 mA. The incident beam was defined by a 1.0 mm diameter collimator and a 0.001 in. Ni filter, with a 1.5 mm

Journal of Polymer Science: Part B: Polymer Physics, Vol. 31, 1331–1337 (1993)
 CCC 0887-6266/93/101331-07

Table I. PET Fibers

Fibers	As Spun Morphology[a]	Density[b]	Degree of Crystallinity[c]	Orientation[b]	
				Crystalline	Amorphous
1W70	Unoriented amorphous	0.282	0.18	0.98	0.86
1W90	Oriented amorphous	0.307	0.22	0.98	0.72
A330	Oriented, slight crystallinity	0.282	0.23	0.98	0.69
EXP	Oriented, moderate crystallinity	0.269	0.24	0.98	0.59

[a] As determined from birefringence and WAXS.[1-3]
[b] g/cc from refs. 1–3.
[c] From NMR.[47]

diameter diffracted beam collimator used to reduce air scatter.

Small-angle X-ray scattering (SAXS) measurements employed a 10 m camera at the National Institute of Standards and Technology.[10] The X-ray source was a 12 kW rotating copper anode operated at 45 kV and 180 mA. A two-dimensional position sensitive detector was used, with a sample-to-detector distance of 2.8 m. A description of the data treatment of the raw images is given elsewhere.[11]

RESULTS AND DISCUSSION

Longitudinal Fiber Structure

The experimental scattering intensities measured for the ($\bar{1}05$) reflection (Figure 1) were fitted to a modified Gaussian–Cauchy equation[12]:

$$I(\theta) = fI_{\max}\exp\left(-2.773\left(\frac{\theta-\theta_{\max}}{\Delta}\right)^2\right) + \frac{(1-f)I_{\max}}{1+\left(\frac{2(\theta-\theta_{\max})}{\Delta}\right)^2} + I_{\text{back}} \quad (1)$$

where $I_{\max}$ is the maximum scattering of a reflection, occurring at a scattering angle $\theta = \theta_{\max}$, and Δ represents the full width of the peak at half-maximum intensity. I_{back} and f are constants for a given reflection. From the value of Δ (in radians) the length of the crystallite in the chain direction $l_{\bar{1}05}$ is obtained using the Scherrer equation[13]:

$$l_{\bar{1}05} = \frac{k\lambda}{\Delta\cos\theta} \quad (2)$$

where k is approximately unity. These $l_{\bar{1}05}$ values are listed in Table II. Equation (2) attributes all smearing of the reflection to finite crystal size, which is true only if there are no crystal defects. The absence of higher order reflections precludes a better analysis, although it has been asserted that lattice imperfections make a negligible contribution to the broadening of the ($\bar{1}05$) reflection in PET.[14]

The SAXS patterns measured from these well-oriented fibers were of the four-point type.[15,16] A long period L for the fibrils was determined from the angular position of the maximum in small-angle scattering parallel to the fiber. As illustrated in Figure 2, the peak of the scattering was fitted to eq. (1) taking $f = 1$, with the data expressed in the Lorentz corrected form[17] (that is, Is^2 vs s, where $s = (2\sin\theta)/\lambda$). On the basis of the Bragg equation,[11,13] the long period is taken to equal the inverse of the s corresponding to the maximum in Is^2, $L = 1/s_{\max}$. The long periods obtained in this manner are listed in Table II.

A longitudinal crystallinity $X_{\parallel}$ can be calculated for each fiber as the ratio of the crystallite c length to the long period:

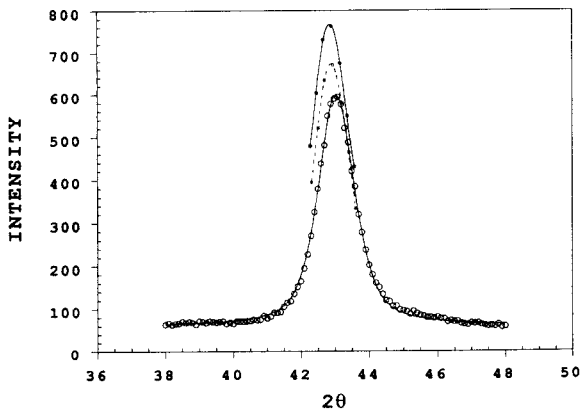

Figure 1. WAXS measured for 1W70 at fiber stresses equal to 0 (OOO), 38 (□□□), and 85 (●●●) MPa respectively, along with the best fit to eq. (1).

Table II. X-Ray Scattering Results for Fiber Structure

Fiber	l_{105}[a]	L[a]	$L - l_{\bar{1}05}$	$X_{\|\|}$	$E_{X\text{-ray}}$[b]	K	$X_{\|\|}K^{-1}$	$X_{\perp}$	D[a]
1W70	75	98	23	0.76	59	1.87	0.41	0.24	79
1W90	74	105	31	0.71	76	1.46	0.49	0.30	123
A330	71	102	31	0.69	63	1.76	0.40	0.33	103
EXP	69	108	39	0.64	61	1.80	0.36	0.37	111

[a] Ångstroms.
[b] GPa.

$$X_{\|} = \frac{l_{\bar{1}05}}{L} \tag{3}$$

The decrease in the crystallite $l_{\bar{1}05}$ dimension and the increasing L both contribute to the systematic decrease in longitudinal crystallinity with increased spinning speed. This indicates a substantial increase at the higher spinning speeds in the average longitudinal dimension of the amorphous regions (see Table II). For equal amorphous orientations, the fiber shrinkage (length change upon relaxation) arising from contraction of the intrafibrillar amorphous chains and tie molecules should parallel the quantity $(L - l_{\bar{1}05})$. Hence, if only the intrafibillar amorphous regions are important, greater shrinkage is anticipated for the HSS fibers. That the HSS fibers actually exhibit greater dimensional stability[1-3] is an indication of the significance of the transverse morphology in governing the physical properties of these fibers.[18]

Transverse Fiber Structure

The apparent crystal modulus $E_{X\text{-ray}}$ of the PET fibers is the apparent crystal modulus determined from the extension of the crystal unit cell in response to an applied stress (Figure 1). The WAXS intensities measured in the meridional direction were fitted to eq. (1) to determine the $(\bar{1}05)$ peak center, with the lattice spacing in the fiber direction then taken as $d = 1/s_{max}$. The X-ray modulus is defined by the ratio of the fiber tension σ_{fib} to the crystal strain ϵ_{cr}

$$E_{X\text{-ray}} \equiv \frac{\sigma_{fib}}{\epsilon_{cr}} = \frac{\sigma_{fib} d_0}{\delta d} \tag{4}$$

where δd is the measured change in lattice spacing. Within experimental error, the d spacing in the absence of stress was the same for all fibers, $d_0 = 2.103$. The change in the spacing of the $(\bar{1}05)$ planes was in all cases proportional to the fiber tension (representative results shown in Figure 3). The X-ray moduli obtained are listed in Table II.

If a homogeneous stress condition prevails (i.e., the fibers are comprised of alternating crystalline and amorphous regions without transverse structural heterogeneity), $E_{X\text{-ray}}$ would be the same for every fiber and equal to the crystal modulus E_{cr}.

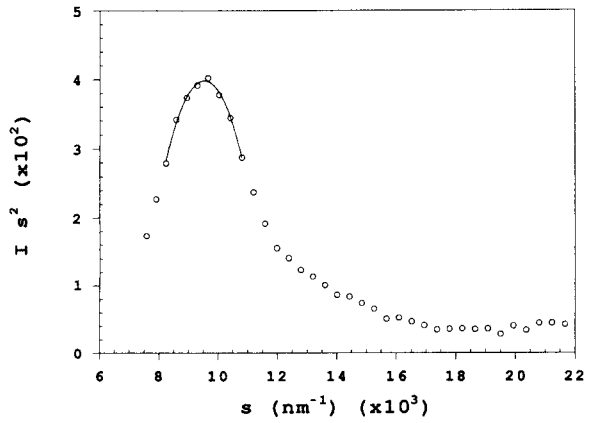

Figure 2. SAXS data in the Lorentz corrected form for 1W70. The angle of maximum intensity, used for the determination of the long period, was obtained from fitting the peak to eq. (1) with $f = 1$.

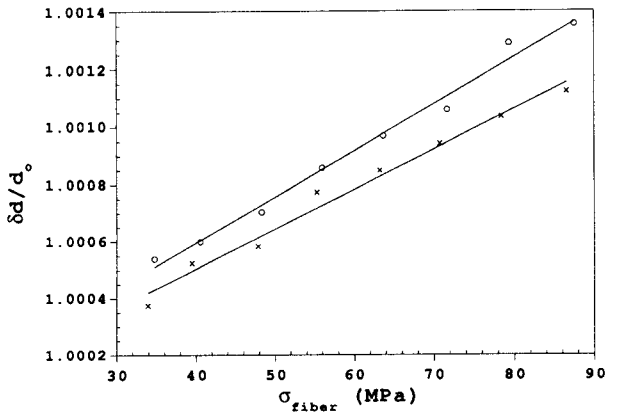

Figure 3. The crystal strain measured for various stresses in 1W90 (×××) and A330 (OOO). Each experimental point represent the average of four separate measurements at that stress.

The accepted value for the crystal modulus is 110 GPa,[6] in accord with theoretical estimates of E_{cr}.[19,20] Consistent with results of other investigations,[6,21,22] $E_{X\text{-ray}}$ is found herein for every fiber to be significantly less than E_{cr}. This observation directly demonstrates that the stress experienced by the crystallites is higher than the applied stress. This is due to the existence of interfibrillar material, which must be lower in modulus than the crystalline phase. Such a morphology results in a concentration of the applied stress on the crystalline phase, such that the apparent crystal modulus obtained from WAXS is less than the actual E_{cr}.

This amplification of stress on the crystallites is given by the ratio

$$K \equiv \frac{E_{cr}}{E_{X\text{-ray}}} \tag{5}$$

a quantity that is related to the fraction of the fiber cross section occupied by fibrils. Specifically, the transverse crystallinity must be less than the reciprocal of the stress intensity factor[22]

$$X_\perp \leq K^{-1} \tag{6}$$

The determination of $E_{X\text{-ray}}$ provides an upper limit to the transverse crystallinity, with the exact relationship between $E_{X\text{-ray}}$ and $X_\perp$ depending on the modulus of the interfibrillar regions.[22] Equality of $1/K$ and $X_\perp$ would correspond to interfibrillar regions unable to support any of the applied stress (e.g., voids). A special case is $K^{-1} = X_\perp = 1$, which implies no interfibrillar amorphous regions.

For the usual circumstance $0 < X_\perp < K^{-1}$, the exact relationship between crystal stress amplification and $X_\perp$ depends on the modulus of the intercrystalline phase, and in fact can be used to determine the latter.[18] The upper bound for $X_\perp$ (i.e., K^{-1}) deduced from eq. (6) is listed in Table II for each fiber. All fibers have substantial interfibrillar noncrystallinity. While this is in agreement with other studies of PET fibers, on occasion X-ray moduli have been reported for PET that equal, or even exceed, the theoretical E_{cr}.[23-25] The samples in these studies were very high in crystallinity, as a result of prolonged annealing at constant length and high temperatures. If the lateral size of the crystallites becomes substantial, stress concentration will be minimized, yielding $E_{X\text{-ray}}$, which approaches E_{cr}. Constant-length annealing effects lateral thickening of the crystallites, and this has been observed to be accompanied by a systematic increase in $E_{X\text{-ray}}$.[26]

A maximum amount of total crystallinity can be calculated from the upper bound on $X_\perp$ obtained from eq. (6):

$$X_{cr} = X_\perp X_\parallel \leq \frac{X_\parallel}{K} \tag{7}$$

This upper bound on X_{cr} is listed in Table II for all fibers. There are various methods by which the total degree of crystallinity of a polymer can be assessed. Unfortunately, for PET there is no correlation among results obtained by different methods.[27-30] To some extent this reflects the fact that different experiments probe different physical features of the material.[30,31]

An easy, and hence popular, method is from determination of the heat of fusion by differential scanning calorimetry (DSC). However, there are serious problems with the use of DSC data for absolute crystallinity determinations in polymers, the most obvious being that the act of measurement disrupts that which is being measured. Particularly for PET, crystallization during the course of the temperature scan can also introduce error. Absolute determinations from DSC require knowledge of the (hypothetical) heat of fusion for a completely crystalline sample, the correct value of which can be in doubt due to crystal defects and the finite crystal size, as well as a significant dependence of the perfect heat of fusion on temperature.[32,33]

The most common method for quantifying the extent of crystallization in a polymer is from the mass density. If a two-phase morphology can be assumed, the degree of crystallinity is deduced from knowledge of the crystal and amorphous densities. Unfortunately, in PET both these quantities are uncertain. From X-ray analysis of the unit cell, many values have been reported for the crystal density of PET, ranging from 1.455[5] to 1.529 g/cc.[34] At least some of this discrepancy may arise from a dependence of the unit cell dimensions on the crystallization conditions. Huisman and Heuvel have reported that the crystalline density of PET is a function of the processing conditions.[35] A similar problem exists with regard to the amorphous density of PET. Since this polymer can be quenched into a completely amorphous state, the density of the amorphous phase (1.335[35]) is well established; however, the amorphous density of PET is a function of orientation.[27,36,37] In fact, it has been found that a density as high as 1.349 can be achieved in completely amorphous PET during spinning.[38] The X_{cr} determined from sample density for the fibers studied herein varies by as much as 100% due to the

uncertainties in both the crystal and amorphous phase densities. Neglecting differences in the fiber orientations, the relative crystallinities deduced from densities are more reliable. Nevertheless, our purposes herein require an accurate absolute determination of X_{cr}, whereby the estimates from sample densities are inutile.

Nuclear magnetic resonance (NMR) has been used for some time for the analysis of crystallinity in PET.[39-43] From fitting the wide-line NMR signal measured above the glass transition temperature to a two-component function, Zachmann[43-45] assessed the concentration of taut tie-molecules in PET. However, this approach relies on the (problematic) determination of X_{cr} by independent means (e.g., density or DSC). More recent ^{13}C-NMR studies of PET fibers suffer the same problem.[42]

Interpretation of NMR experiments in terms of the quantity of crystalline and amorphous phases present is confounded by spin diffusion. Especially for small domain sizes, spin diffusion can blur the contributions from different phases to the measured free induction decay. This problem is avoided with a newer NMR technique in which spin diffusion is quenched by multiple pulse radiofrequency irradiation.[46] The measured spin-lattice relaxation behavior is sensitive to both the amplitude and frequency of motions, allowing domains in the heterogenous PET morphology to be defined according to their mobility. The use of a multiple-pulse sequence is more effective in quenching spin diffusion than conventional NMR methods, thus providing more accurate morphological information.[46] More recently, this NMR method was successfully applied to PET films and fibers of various orientations and crystallinities, including the fibers of the present study.[47]

Since multiple-pulse proton NMR provides an absolute measure of crystallinity, not based on any a priori assumptions concerning the fiber morphology, it was the method used herein for determination of the degree of crystallinity. Moreover, an independent test of the NMR method is available; the degree of crystallinity must be consistent with the upper bound on X_{cr} deduced from eq. (7). This is indeed the case (Table I), supporting the claim[46,47] that this NMR experiment provides a more accurate measure of X_{cr}.

Since the total crystallinity is simply the product of the longitudinal and transverse degrees of crystallinity, a value for the degree of crystallinity in the direction perpendicular to the fibrils can be deduced from X_{cr} and $X_{||}$ (eq. 7). These results (using the NMR determination of X_{cr}) are tabulated in Table II. The interfibrillar amorphous content is substantial in all fibers, with only about one-third of the fiber cross section occupied by fibrils. While a longitudinal crystallinity equal to unity is obviously unlikely for flexible chain polymers such as PET, it is evident that extensive crystallization perpendicular to the fibrils is also suppressed. This transverse degree of crystallinity increases with spinning speed, consistent with the smaller stress concentration factor (higher $E_{X\text{-ray}}$) measured for the HSS fibers (Table II).

From the breadth of the SAXS peak in the transverse direction (Figure 4) the fibril diameter can be determined. Neglecting any contribution to the smearing from lattice imperfections (e.g., defects, paracrystallinity, waviness), the average fibril diameter is given by[48]

$$D = 1.04 \frac{\lambda}{\Delta} \tag{8}$$

The obtained values of D are listed in Table II for all fibers. It is seen that HSS is associated with an increased fibril diameter. High-speed spinning of PET is known to effect orientational crystallization in the spin line.[4,49-52] Due to the consequently higher temperature of crystallization, larger crystallite sizes are expected. This is consistent with a larger D and may account for the higher melting points of the HSS fibers.[1-3]

The significant increase in fiber diameter for the HSS fibers is not accompanied by a proportional increase in the transverse degree of crystallinity. This suggests a systematic reduction in the concentration of fibrils for HSS, consistent with reduced nucleation at higher crystallization temperatures.[4,53]

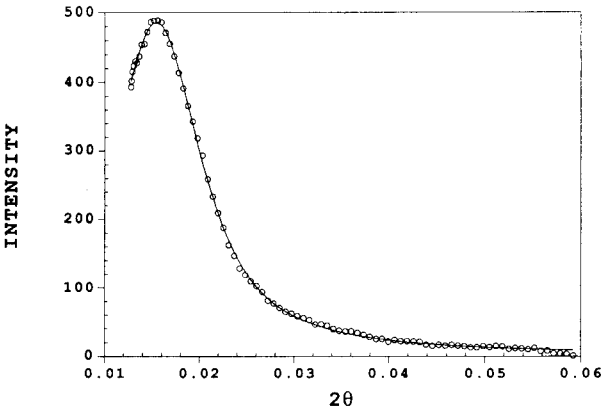

Figure 4. SAXS for 1W90 used to determine the fibril diameter. Data were measured along the transverse direction of a circularly averaged lobe of the four-point pattern.

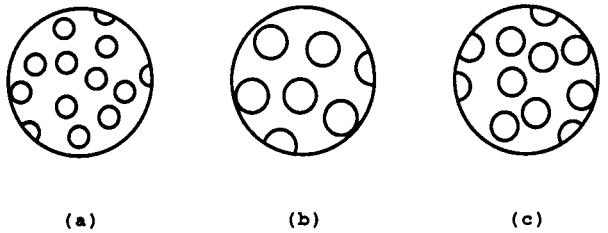

Figure 5. Schematic of cross section of filaments indicating the relative size of fibrils and the interfibrillar distances for (a) 1W70, (b) 1W90, and (c) A330.

As illustrated in Figure 5, this implies greater lateral separation of the fibrils for HSS, which presumably exerts a significant effect on physical properties.[18]

SUMMARY

Both the measured $E_{X\text{-ray}}$ and the transverse crystallinities deduced for the fibers demonstrate the gross inadequacy of a two-phase fibrillar model in describing the structure of PET fibers. Only about one-third of the fiber cross section is actually occupied by crystalline material. In comparison to conventional spinning, the HSS fibers exhibit higher transverse crystallinities, and correspondingly smaller stress concentrations on their crystalline phases. This trend is also evident in the larger fibril diameters measured for the HSS fibers. It appears there may be a concomitant reduction in the number density of fibrils, however, such that the specific surface area of the fibrils may decrease for HSS. The effect of the transverse structural changes accompanying HSS on the mechanical properties of PET fibers is assessed in the ensuing paper.[18]

This work was supported by the Allied-Signal Corp. and the Office of Naval Research. The assistance of Drs. W. W. Adams and H. H. Song of the Air Force Wright Laboratory (WAXS) and Dr. J. Barnes of NIST (SAXS) is gratefully acknowledged. DWT acknowledges support from the National Research Council by an NRC-NRL postdoctoral fellowship.

REFERENCES AND NOTES

1. P. B. Rim and C. J. Nelson, *J. Appl. Polym. Sci.*, **42,** 1807 (1991).
2. P. B. Rim and C. J. Nelson, *J. Tex. Inst.*, **83,** 78 (1992).
3. P. B. Rim and C. J. Nelson, *Rubber World,* **204,** 30 (1991).
4. A. Ziabicki and H. Kawai, (eds.), *High-Speed Fiber Spinning,* Wiley, New York, 1985.
5. R. de P. Daubeny, C. W. Bunn, and C. J. Brown, *Proc. Roy. Soc. (London),* **A226,** 531 (1959).
6. T. Thistlewaite, R. Jakeways, and I. M. Ward, *Polymer,* **29,** 61 (1988).
7. J. H. Dumbleton and B. B. Bowles, *J. Polym. Sci. Part A-2,* **4,** 951 (1966).
8. P. G. Lenhert and W. W. Adams, *A User's Manual for Fiber Diffraction: The Automated Picker and Huber Diffractometers,* Materials Laboratory, Wright Research and Development Center, Final Report 1986–90, WRDC-TR-90-4069 (1990).
9. P. G. Lenhert and W. W. Adams, *Tensile Modulus by X-Ray Diffraction: Instrument and Method,* Materials Laboratory, Wright Research and Development Center, Final Report 1986–90, WRDC-TR-90-4069 (1990).
10. R. W. Hendricks, *J. Appl. Cryst.,* **11,** 15 (1978).
11. M. Meyers, A. Wims, T. Ellis, and J. Barnes, *Macromolecules,* **23,** 2807 (1990).
12. A. M. Hindeleh and D. J. Johnson, *Polymer,* **19,** 27 (1978).
13. L. E. Alexander, *X-Ray Diffraction Methods in Polymer Science,* R. E. Krieger Publishing Co., Malabar, Florida, 1985.
14. E. W. Fischer and S. Fakirov, *J. Mat. Sci.,* **11,** 1041 (1976).
15. R. J. Matyi and B. Crist, *J. Polym. Sci., Poly. Phys. Ed.,* **16,** 1329 (1978).
16. R. J. Matyi and B. Crist, *J. Macromol. Sci. Phys.,* **B16,** 15 (1979).
17. B. Crist and N. Morosoff, *J. Polym. Sci., Polym. Phys. Ed.,* **11,** 1023 (1973).
18. K. L. Peng and C. M. Roland, *J. Polym. Sci., Polym. Phys. Ed.,* **31,** 1339 (1993).
19. K. Tashiro, M. Kobayashi, and H. Tadokoro, *Macromolecules,* **10,** 413 (1977).
20. L. R. G. Treloar, *Polymer,* **1,** 279 (1960).
21. I. Sakurada, T. Ito, and K. Nakamae, *J. Polym. Sci. C,* **15,** 75 (1966).
22. L. I. Slutsker, W. W. Adams, and C. M. Roland, *Polym. Prepr.,* **33(1),** 317 (1992).
23. I. Sakurada and K. Kaji, *J. Polym. Sci. C,* **31,** 57 (1970).
24. K. Nakamae, T. Nishino, F. Yokoyama, and T. Matsumoto, *J. Macromol. Sci. Phys.,* **B27,** 407 (1988).
25. W. J. Dulmage and L. E. Contois, *J. Polym. Sci.,* **28,** 275 (1958).
26. L. I. Slutsker, unpublished results.
27. G. Farrow and I. M. Ward, *Polymer,* **1,** 330 (1960).
28. W. O. Statton, *J. Appl. Polym. Sci.,* **7,** 803 (1963).
29. F. Fontaine, J. Ledent, G. Groeninckx, and H. Reynaers, *Polymer,* **23,** 185 (1982).
30. S. Fakirov, E. W. Fischer, R. Hoffmann, and G. F. Schmidt, *Polymer,* **18,** 1121 (1977).
31. D. E. Bosely, *J. Appl. Polym. Sci.,* **8,** 1521 (1964).
32. A. Peterlin and G. Meinel, *J. Polym. Sci.,* **B3,** 783 (1965).

33. A. Mehta, U. Gaur, and B. Wunderlich, *J. Polym. Sci., Polym. Phys. Ed.*, **16,** 289 (1978).
34. M. G. Northolt and H. A. Stuut, *J. Polym. Sci., Polym. Phys. Ed.*, **16,** 940 (1978).
35. R. Huisman and H. M. Heuvel, *J. Appl. Polym. Sci.*, **22,** 943 (1978).
36. J. H. Nobbs, D. I. Bower, and I. M. Ward, *Polymer*, **17,** 25 (1976).
37. C. M. Roland and M. F. Sonnenschein, *Polym. Eng. Sci.*, **31,** 1434 (1991).
38. H. M. Heuvel and R. Huisman in ref. 4, p. 295.
39. A. Cunningham, A. J. Manuel, and I. M. Ward, *Polymer*, **17,** 126 (1976).
40. M. D. Sefcik, J. Schaefer, E. O. Stejskal, and R. A. McKay, *Macromolecules*, **13,** 1132 (1980).
41. A. D. English, *Macromolecules*, **17,** 2182 (1984).
42. D. L. Tzou, P. Seai, A. S. Abhiraman, T.-H. Huang, *J. Polym. Sci., Poly. Phys.*, **29,** 49 (1991).
43. U. Eichhoff and H. G. Zachmann, *Makromol. Chem.*, **147,** 41 (1971).
44. H. J. Biangardi and H. G. Zachmann, *J. Polym. Sci., Polym. Symp.*, **58,** 169 (1977).
45. H. G. Zachmann, *Poly. Eng. Sci.*, **19,** 966 (1979).
46. J. R. Havens and D. L. VanderHart, *Macromolecules*, **18,** 1663 (1985).
47. J. H. Walton, J. B. Miller, and C. M. Roland, to be published.
48. B. Crist, *J. Appl. Cryst.*, **12,** 27 (1979).
49. H. M. Heuvel and R. Huisman, *J. Appl. Polym. Sci.*, **22,** 2229 (1978).
50. P. Desai and A. S. Abhiraman, *J. Polym. Sci., Polym. Phys. Ed.*, **26,** 1657 (1988).
51. H. A. Hristov and J. M. Schultz, *J. Polym. Sci., Polym. Phys. Ed.*, **28,** 1647 (1990).
52. J. M. Schultz, *Polym. Sci. Eng.*, **31,** 661 (1991).
53. H. H. George, A. Holt, and A. Buckley, *Polym. Eng. Sci.*, **23,** 95 (1983).

Received June 1, 1992
Accepted December 30, 1992